PROCEEDINGS OF SCIENCE

The BESS-Polar II lower-energy antiproton flux using the upper-middle TOF trigger mode

K. Sakai [*],[a,b,*] **K. Abe** [†],[c] **H. Fuke,**[d] **S. Haino** [‡],[e] **T. Hams,**[a,b] **M. Hasegawa,**[e] **H. Jeon,**[a,b] **K. C. Kim,**[f] **M. H. Lee** [§],[f] **Y. Makida,**[e] **J. W. Mitchell,**[a] **J. Nishimura,**[d,g] **M. Nozaki,**[e] **R. Orito** [¶],[h] **J. F. Ormes,**[i] **M. Sasaki,**[a,b] **E. S. Seo,**[f] **R. E. Streitmatter** [‖],[a] **N. Thakur** [**],[a] **A. Yamamoto,**[e] **T. Yoshida**[d] **and K. Yoshimura**[j]

[a] *NASA-Goddard Space Flight Center (NASA-GSFC), Greenbelt, MD 20771, USA*
[b] *Center for Research and Exploration in Space Science and Technology (CRESST)*
[c] *Kobe University, Kobe, Hyogo 657-8501, Japan*
[d] *Institute of Space and Astronautical Science, Japan Aerospace Exploration Agency (ISAS/JAXA), Sagamihara, Kanagawa 252-5210, Japan*
[e] *High Energy Accelerator Research Organization (KEK), Tsukuba, Ibaraki 305-0801, Japan*
[f] *IPST, University of Maryland, College Park, MD 20742, USA*
[g] *The University of Tokyo, Bunkyo, Tokyo 113-0033, Japan*
[h] *Kobe University, Kobe, Hyogo 657-8501, Japan*
[i] *University of Denver, Denver, CO 80208, USA*
[j] *Okayama University, Okayama, Okayama 700-8530, Japan*

E-mail: kenichisakai@uchicago.edu

To observe cosmic-origin antiparticles, it is crucial to mitigate the astrophysical background. One approach involved searching for background-free antideuterons/antihelium; however, no viable candidates were identified. Consequently, we extended our antiproton observations to the lower-energy region below 0.2 GeV, where the contribution from secondary particles is minimized, and explored the potential signatures of dark matter in the 4.7×10^9 cosmic ray events recorded by BESS-Polar II during the solar activity minimum in 2007. We modified the trigger conditions to utilize the middle time-of-flight (TOF), effectively reducing the amount of passing material by half. We will report the details of the analysis and the lower-energy antiproton flux measured by BESS-Polar II.

39th International Cosmic Ray Conference (ICRC2025)
15–24 July 2025
Geneva, Switzerland

[*]Present address: Enrico Fermi Institute of The University of Chicago, Chicago, IL 60637, USA.
[†]Present address: Kamioka Observatory, Institute for Cosmic Ray Research, the University of Tokyo, Higashi-Mozumi, Kamioka, Hida, Gifu 506-1205, Japan.
[‡]Present address: Institute of Physics, Academia Sinica, Nankang, Taipei 11529, Taiwan.
[§]Present address: Center for Underground Physics, Institute for Basic Science (IBS), Daejeon 34126, Korea.
[¶]Present address: Tokushima University, Tokushima 770-8506, Japan.
[‖]Deceased.
[**]Present address: Prince George's Community College, Largo, MD 20774, USA.
[*]Speaker

PoS(ICRC2025)126

1. Introduction

The possible presence of various species of antimatter in the cosmic radiation can provide evidence of sources and processes important for both astrophysics and elementary particle physics. Most of the observed cosmic-ray antiprotons ($\bar{p}$'s) are well understood as secondary products of collisions between primary cosmic-rays and the interstellar medium. The energy spectrum of such "secondary" $\bar{p}$'s peaks near 2 GeV, and decreases sharply below and above the peak, due to the kinematics of $\bar{p}$ production and to the local interstellar (LIS) proton spectrum. Cosmologically "primary" sources have been suggested, including the annihilation of dark-matter (DM) particles and the evaporation of primordial black holes (PBH) by Hawking radiation [1]. Before the BESS experiment, the detection of the peak in the secondary $\bar{p}$ spectrum and the search for a possible low-energy primary $\bar{p}$ component had not been realized, because of huge backgrounds and the extremely small flux, especially at low energies.

2. BESS Program

The BESS instrument [2, 3] was developed as a high-resolution magnetic-rigidity spectrometer for cosmic-ray antiparticles and precise measurements of the absolute fluxes of various cosmic-ray components. The original BESS experiment performed 9 flights over northern Canada during the period of 1993 through 2002 with continuous improvement in the instrument. The BESS-Polar project was proposed as an advanced BESS program using long duration balloon (LDB) flights over Antarctica (around the south pole) to provide high-statistics, low-energy cosmic-ray measurements [4–6]. The first scientific flight of the BESS-Polar instrument was launched near US McMurdo Station in Antarctica, on December 13th, 2004 (UTC). The flight duration was over 8.5 days and more than 9×10^8 cosmic-ray events were recorded [7]. Incorporating considerable improvements in instrument and payload systems compared to BESS-Polar I, the BESS-Polar II instrument was launched on December 23, 2007, from Williams Field near the McMurdo Station and circulated around the South Pole for 24.5 days of observation with the magnet energized. The float altitude was 34 km to 38 km (residual air of 5.8 g/cm^2 on average), and the cutoff rigidity was below 0.5 GV. BESS-Polar II accumulated 4.7×10^9 events with no inflight event selection as 13.6 terabytes of data (Figure 1).

Figure 1: Flight trajectories of the 2007 BESS-Polar II over Antarctica from Williams Field (first orbit blue, second orbit red) with 2004 BESS-Polar I flight (green).
[Launch]S77-51,E166-40, 06:27(McM) 12/23 2007
[Recovery]S83-51,W073-04, 09:02(UTC) 1/21 2008

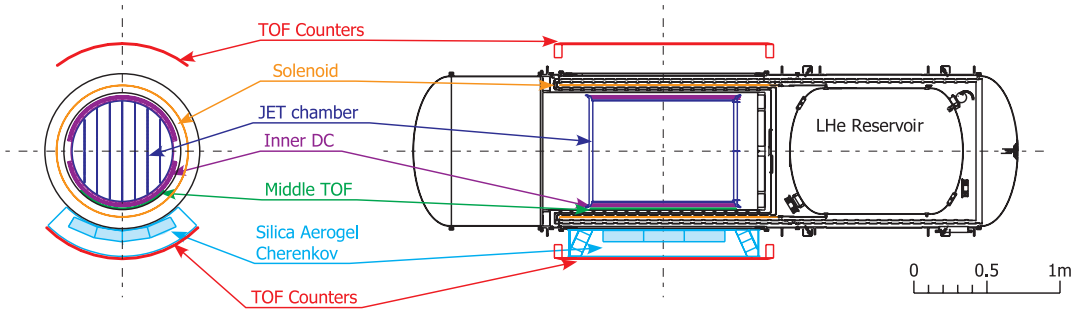

Figure 2: Cross-section and side views of the BESS-Polar II instrument. In the side view, the LHe reservoir is installed on the right side, with the electronics installed on the opposite side.

Previous studies utilizing BESS-Polar II data have led to the publication of results for $\bar{p}$ [8] and antihelium ($\overline{\text{He}}$) [9] in Physical Review Letters (PRL) in 2012 and for proton (p) and helium (He) fluxes in the Astrophysical Journal (APJ) in 2016 [10]. Most recently, the results of an antideuteron ($\bar{d}$) search were published in PRL in 2024 [11].

3. BESS-Polar Instrument

The BESS-Polar II instrument, as shown in Figure 2, provides a uniform magnetic field using a thin superconducting solenoid magnet, 0.9 m in diameter and 1.4 m in length. The superconducting magnet utilizes NbTi/Cu wire with a high-strength aluminum stabilizer, incorporating Ni-doped filaments to enhance its strength. The magnet and cryostat have a minimal material thickness of 2.46 g/cm^2 per wall. In BESS-Polar II, the magnet operates in persistent mode with a cryogen hold time of 25 days, using a 520-liter liquid helium (LHe) reservoir. This magnet operates stably at 1 Tesla (1 T), although during both flights, it was operated at 0.8 T to provide an additional margin of stability.

A central jet-cell drift chamber tracking system (JET), along with inner drift chambers (IDC), provides 52 trajectory points with 125 μm resolution in the bending direction and is situated inside the warm bore of the solenoid. In the non-bending direction, vernier pads in each layer of the IDCs accomplish 650 μm resolution, and JET measurements using charge division give 24 mm. These detectors measure the trajectories of charged particles as they pass through the magnetic field. The magnetic rigidity, $R = pc/Ze$ (where p is the momentum, c is light speed and Ze is the particle's electric charge), is determined by fitting the curvature of the track within the magnetic field. The MDR is 240 GV with a uniform magnetic field of 0.8 T. The charge sign of an incident particle is determined by the direction of its curved track.

Arrays of time-of-flight (TOF) scintillators are positioned at the top (UTOF) and bottom (LTOF) of the instrument, while middle TOF (MTOF) is located inside the magnet bore beneath the lower IDC. The TOF scintillators trigger event readout and measure the charge and velocity (β) of the incident particles. The timing resolution for p is 120 ps, resulting in β^{-1} resolution of 2.5% in UTOF-LTOF trigger events, and 320 ps, yielding β^{-1} resolution of 8.5% for UTOF-MTOF trigger events. Particle momentum is derived from the rigidity and charge, and, in turn, particle mass is calculated from momentum and β. BESS-Polar can resolve $\bar{p}$'s by mass to an energy of 1.5 GeV.

To extend $\bar{p}$ measurements to approximately 3.6 GeV, an aerogel Cherenkov counter (ACC) with an index n = 1.03 is positioned below the cryostat to reduce the overwhelming background from light, high-energy μ^-'s, and e^-'s by a factor of over 11000.

4. Scientific Motivation for Low-Energy $\bar{p}$'s and Highlights from the BESS-Polar II results

Cosmic-ray antinuclei, including $\bar{p}$'s, $\overline{\text{He}}$, and $\bar{d}$'s, are crucial for understanding the early universe. They serve as unique probes sensitive to DM and local PBHs, extending beyond the standard model.

The BESS-Polar II $\bar{p}$ measurement [8] was motivated by the observation of a slightly flatter low-energy $\bar{p}$ flux in the BESS95+97 flights [12], compared to predictions based on secondary $\bar{p}$ production from collisions between high-energy cosmic rays and ISM. This discrepancy may indicate the existence of novel cosmic-ray $\bar{p}$ production in the Universe, such as the evaporation of PBH [15]. Figure 3 shows the BESS-Polar II $\bar{p}$ flux with BESS95+97, PAMELA [13], AMS-02 measurements [14] and solar-minimum secondary calculations. Precise measurements of the $\bar{p}$ fluxes were conducted during the BESS-Polar II flight, which detected approximately 8,000 $\bar{p}$'s in the energy range from 0.17 to 3.5 GeV [8]. Meanwhile, PAMELA detected around 1,500 events in the range of 0.06 to 180 GeV [13]. The $\bar{p}$ fluxes calculated in both experiments agree within the combined statistical and systematic uncertainties. In the higher rigidity region from 1 to 450 GV, AMS-02 reported a high-statistics $\bar{p}$ flux with an integrated 3.49×10^5 events [14]. The AMS-02 results suggest a potential excess that is consistent with DM having a mass between 20 and 80 GeV, while also aligning with expectations from secondary production within theoretical uncertainties. Therefore, in the energy range where measurements have been conducted, significant improvements in both statistical and systematic uncertainties are essential for identifying primary $\bar{p}$'s, over the large background of secondary $\bar{p}$'s.

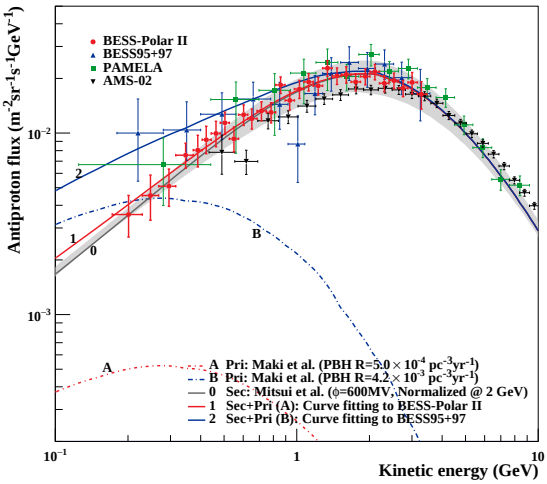

Figure 3: BESS-Polar II $\bar{p}$ flux [8] at solar minimum with others [12–14]

In contrast, at low energies, the secondary-origin $\bar{p}$ flux, which peaks around 2 GeV, is kinematically suppressed. As a result, any potential DM signature could appear as an excess in this region. Notably, the improved statistical precision of the $\bar{p}$ flux measured using UTOF-LTOF trigger events in BESS-Polar II stems from the significantly larger number of events below 1 GeV: approximately 14 times more than in BESS95+97, 30 times more than in PAMELA, and more than twice as many as in AMS-02. Nonetheless, further extending the measurement into even lower energy regions is necessary to fully explore possible DM contributions.

In magnetic spectrometer experiments, the mass resolution at low energies is primarily limited by multiple scattering. In this context, the BESS-Polar spectrometer, featuring a gas tracking chamber with significantly less material than silicon-based trackers, combined with a strong mag-

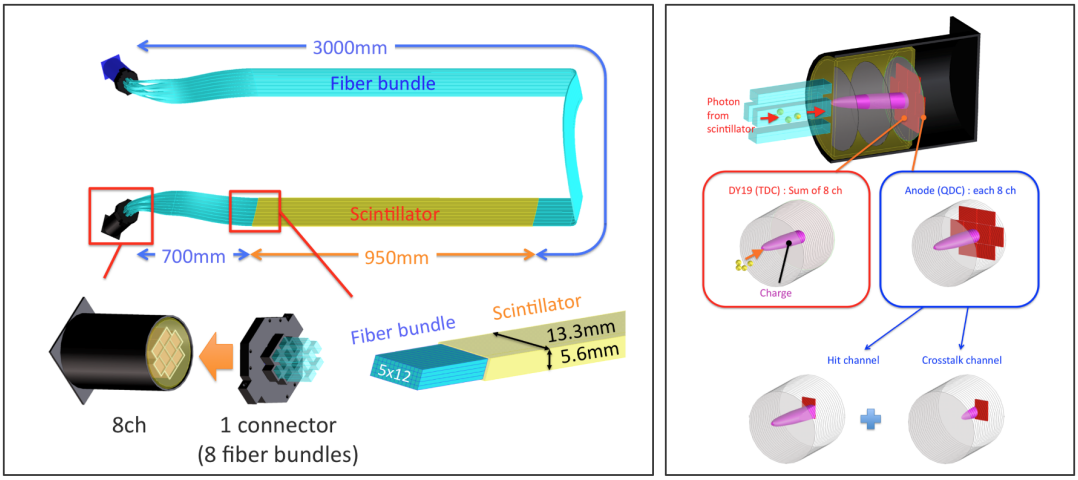

Figure 4: [Left] Overview of the BESS-Polar II MTOF. 8 fiber bundles from the scintillator strips are combined into a single connector, which is attached to the PMT. The total length of the MTOF is 4.65 m. [Right] Schematic view of the MTOF readout. One DY19th dynode signal is used for the TDC, while 8 anode signals are used for the QDC. The hit channels within a single PMT are identified using the QDC information.

netic field provided by a superconducting magnet, offers an optimal configuration for low-energy $\bar{p}$ measurements.

5. Middle TOF Calibration and Analysis

In addition to the UTOF and LTOF counters, a newly developed thin detector, MTOF, was installed in the lower half of the solenoid bore to detect low-energy $\bar{p}$'s. MTOF consists of 48

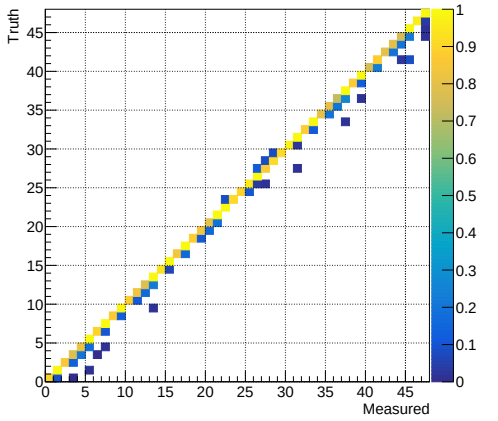

Figure 5: Heatmap of the crosstalk matrix on the reservoir side. The x-axis represents the measured ADC values, while the y-axis indicates the true ADC values.

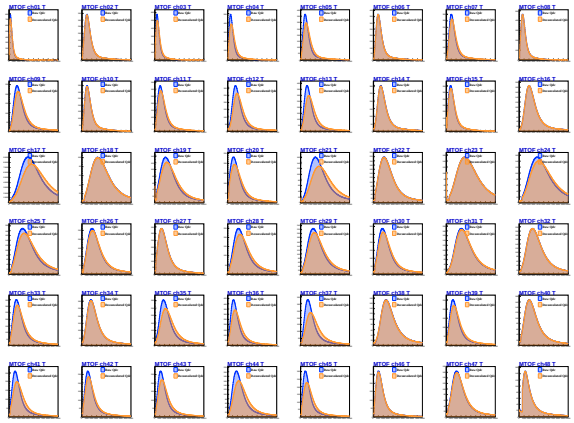

Figure 6: Original (blue) and deconvoluted (orange) charge for reservoir-side PMT 48 using crosstalk matrix.

plastic scintillator bars, each with a cross section of $5.6 \times 13.3\,\mathrm{mm}^2$. These bars are read out from both ends using 8 anode photomultiplier tubes (Hamamatsu R6504MODX-M8), via clear fiber light guides (KURARAY CLEAR-PS, 1.0 mm square). The fiber lengths used in BESS-Polar II are approximately 700 mm and 3000 mm. The overall structure of the MTOF is determined by spatial constraints within the spectrometer and the installation design. Figure 4 shows an overview of the BESS-Polar II MTOF system [16].

The output signals from each TOF counter are used for two purposes: time-of-flight is measured using the 19th dynode signals, which are common to each PMT and routed through an inverting amplifier (gain of 10, bandwidth >1 GHz) to TDC modules with a discriminator threshold of 160 mV (about 5% of the dynode pulse height for MIPs), while dE/dx is measured using 8-channel anode signals read out by QDC modules, with the hit channel determined from the QDC values of each PMT. All TOF PMTs are adjusted so that their axes are as parallel as possible to the magnetic field leakage at the installation location. Any misalignment from perfect parallelism reduces the projected area of the photocathode, which affects the measurement. However, in the case of the MTOF's 8 anode PMTs, such misalignment can lead to crosstalk between channels, resulting in a maximum signal mixing of approximately 20%.

When crosstalk at the 20% level is present, it can generate spurious hits alongside the true signals, which complicates the analysis. To address this, we constructed a crosstalk matrix, as shown in Figure 5, and used it to calculate the deconvoluted charge distribution (see Figure 6). A new calibration was then performed based on these deconvoluted values.

6. $\bar{p}$ Analysis Using the UTOF-MTOF trigger Events

The analysis of the MTOF using single-track data, along with the preliminary particle identification and flux calculation for $\bar{p}$, have been successfully completed. Figure 7 illustrates a lower stopping energy in the flight data when transitioning from LTOF to MTOF, and Figure 8 shows the β^{-1} vs R plot for $|Z| = 1$ particle identification of UTOF-MTOF trigger events in the BESS-Polar

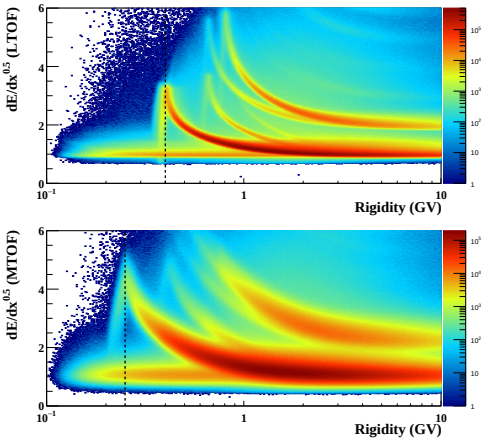

Figure 7: dE/dx vs R plot (top: LTOF, bottom: MTOF). The lines indicate the stopping energy for each.

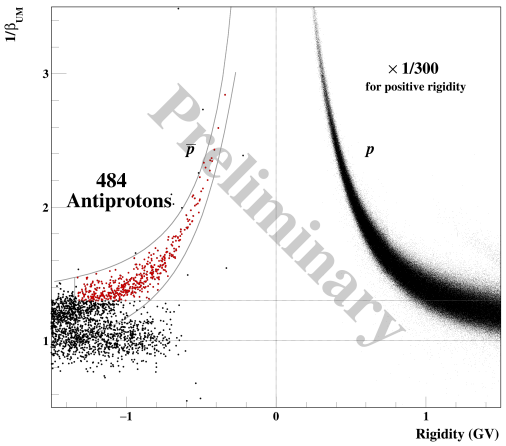

Figure 8: Preliminary $|Z| = 1$ particle ID of single-track events triggered by UTOF-MTOF in the BESS-Polar II data.

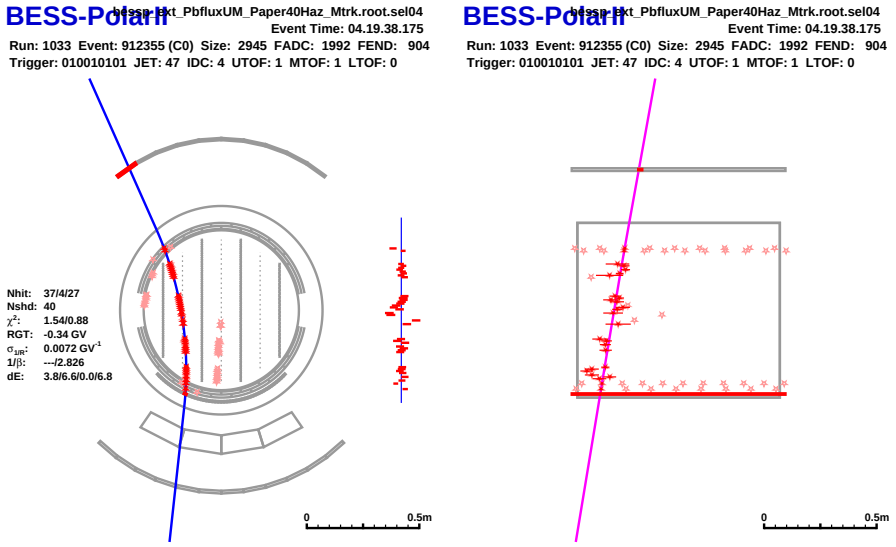

Figure 9: Event display of $\bar{p}$ candidate at the lowest energies ever measured, enabled by the introduction of MTOF

II. To prevent background contamination from e^- and μ^-, $\bar{p}$ candidates with a β^{-1} value below the threshold of 1.3 were rejected, effectively excluding approximately 99.7% of the background. Each time the correction and analysis are refined, hot spots are eliminated, fiducially masked regions are recovered, and the resulting number of identified $\bar{p}$'s increases. However, the resolution of the MTOF has not been finalized, and detailed calibration is required.

As a demonstration of the MTOF's ability to extend $\bar{p}$ identification into the low-energy region, an event display of the lowest-energy $\bar{p}$ observed to date is shown in Figure 9. The backward-going tracks produced by particle annihilation do not enter the tracker region, resulting in a clean single track. However, it can be seen that the particles annihilated after passing through the MTOF and did not reach the LTOF.

7. Conclusion

With continued progress in the MTOF analysis, additional fiducial regions became available, resulting in the identification of 484 $\bar{p}$'s in UTOF-MTOF trigger events.

Acknowledgements

The BESS-Polar collaboration was supported in Japan by MEXT/JSPS grants KAKENHI (JP13001004; JP18104006; JP19340070; JP22540322), and in the U.S. by NASA (NNX08AC18G; NNX08AD70G; NNX10AC48G; NNX10AG32A; NNX12AH13G; NNX12AI66A). The NASA Columbia Scientific Balloon Facility and the National Science Foundation United States Antarctic Program carried out balloon flight operations. We express our sincere thanks for their continuous, professional support.

References

[1] S. W. Hawking, Particle creation by black holes, Commun. Math. Phys. **43**, 199 (1975).

[2] Y. Ajima *et al.*, A superconducting solenoidal spectrometer for a balloon-borne experiment, Nucl. Instrum. Methods Phys. Res. A **443**, 71 (2000).

[3] S. Haino *et al.*, Progress of the bess superconducting spectrometer, Nucl. Instrum. Methods Phys. Res. A **518**, 167 (2004).

[4] A. Yamamoto *et al.*, Bess and its future prospect for polar long duration flights, Adv. Space Res. **30**, 1253 (2002).

[5] J. Mitchell *et al.*, The bess program, Nucl. Phys. B Proc. Suppl. **134**, 31 (2004).

[6] T. Yoshida *et al.*, Bess-polar experiment, Adv. Space Res. **33**, 1755 (2004), the Next Generation in Scientific Ballooning.

[7] K. Abe *et al.*, Measurement of the cosmic-ray low-energy antiproton spectrum with the first bess-polar antarctic flight, Physics Letters B **670**, 103 (2008).

[8] K. Abe *et al.*, Measurement of the cosmic-ray antiproton spectrum at solar minimum with a long-duration balloon flight over antarctica, Phys. Rev. Lett. **108**, 051102 (2012).

[9] K. Abe *et al.*, Search for antihelium with the bess-polar spectrometer, Phys. Rev. Lett. **108**, 131301 (2012).

[10] K. Abe *et al.*, MEASUREMENTS OF COSMIC-RAY PROTON AND HELIUM SPECTRA FROM THE BESS-POLAR LONG-DURATION BALLOON FLIGHTS OVER ANTARCTICA, Astrophys. J. **822**, 65 (2016).

[11] K. Sakai *et al.*, Search for antideuterons of cosmic origin using the bess-polar ii magnetic-rigidity spectrometer, Phys. Rev. Lett. **132**, 131001 (2024).

[12] S. Orito *et al.*, Precision measurement of cosmic-ray antiproton spectrum, Phys. Rev. Lett. **84**, 1078 (2000).

[13] O. Adriani *et al.*, Pamela results on the cosmic-ray antiproton flux from 60 mev to 180 gev in kinetic energy, Phys. Rev. Lett. **105**, 121101 (2010).

[14] M. Aguilar *et al.*, Antiproton flux, antiproton-to-proton flux ratio, and properties of elementary particle fluxes in primary cosmic rays measured with the alpha magnetic spectrometer on the international space station, Phys. Rev. Lett. **117**, 091103 (2016).

[15] K. Maki, T. Mitsui, and S. Orito, Local flux of low-energy antiprotons from evaporating primordial black holes, Phys. Rev. Lett. **76**, 3474 (1996).

[16] A. Horikoshi, Development of a thin scintillation counter hodoscope for detecting the lowest energy cosmic-ray antiprotons, Ph.D. thesis, 2009.